

Contents lists available at ScienceDirect

Energy

journal homepage: www.elsevier.com/locate/energy



Check for updates

Techno-economic assessment of hythane-fueled industrial SOFC systems

Robert Styn ^{a,*} , Hannes Jakob Reichelt ^a , Ralf Peters ^a, Thomas Ernst Müller ^b

- ^a Forschungszentrum Jülich GmbH, Wilhelm-Johnen-Straβe, 52425, Jülich, Germany
- b Ruhr-Universität Bochum, Faculty of Mechanical Engineering Carbon Sources and Conversion, Universitätsstraße 150, 44801, Bochum, Germany

ARTICLE INFO

Keywords:
Fuel cells
SOFC systems
Hythane
Techno-economic assessment
Hydrogen blending
Scale-up
Industrial decarbonization

ABSTRACT

Solid oxide fuel cell (SOFC) systems offer high-efficiency conversion of the chemical energy of fuel gases into electrical energy. To meet market and policy targets, such systems must be able of operating on an industrial scale and be compatible with environmentally friendly fuels. This study models the scale-up of a 750 W natural-gas-fueled SOFC to a 240 kW system with various gas-path configurations, evaluating the impact of blending up to 30 vol% of hydrogen (H_2) into the methane feed. Aspen Plus simulations, coupled with pressure-loss and carbon-deposition models, were used to optimize recirculation ratio and reactant utilization for maximum efficiency. The parallel configuration achieved the highest electrical efficiency of 64.0 %, while series-connected and intermediate systems suffered from increased pressure losses. H_2 admixture simulations confirm that operation is feasible without loss of efficiency in the small- and large-scale systems due to reduced carbon-deposition potential. A techno-economic analysis indicates a 91.7 % cost reduction through scale-up, and a 1.6 % cost increase for adjusting the system to H_2 admixtures. The economic viability of the large-scale system was evaluated for all tested fuel compositions (0.201–0.204 ℓ /kWh), with payback times under 20 years at market-relevant electricity prices. These results demonstrate the technical and economic feasibility of large-scale, H_2 -adapted SOFC systems for industrial decarbonization.

1. Introduction

Greenhouse gas (GHG) emissions from private, public and industrial sectors are a major cause of climate change [1]. In 2019, the energy, industry, transport and building sectors accounted for 79 % of global GHG emissions [2]. In 2021, fossil fuels supplied 81 % of global energy demand (31 % oil, 27 % coal, and 23 % natural gas) [3]. To reduce GHG emissions, particularly CO2, it is necessary to replace fossil energy sources with renewable energy, or to adopt more sustainable energy carriers [4]. The latter also helps overcome the challenges associated with the fluctuating nature of renewable energy [5]. One option is to utilize electricity from solar, wind or hydropower stations to produce green hydrogen [6]. H₂ can be stored and used at the production site [7] or transported via pipelines to the end users [8], similar to natural gas (NG). International commitments, such as the hydrogen strategy of the European Union [9], and initiatives like the European Hydrogen Backbone (EHB) [10] demonstrate the motivation of building a nationwide hydrogen infrastructure. As we transition towards a hydrogen economy [11], the existing NG infrastructure can be used to distribute the hydrogen by blending it into the grid. The mixture of hydrogen and natural gas, often referred to as hythane, and its transportation via pipeline is the focus of several European projects and research [12]. For example, the Deutscher Verein des Gas-und Wasserfaches e.V. (DVGW) and the Avacon AG showed the successful blending of hydrogen at concentrations of up to 20 vol% in a medium pressure part net with 35 km of pipeline and 350 customers [13]. Even though the potential of reducing the GHG emissions through blending is estimated to be between 1 and 2 % [14], this approach has a positive impact on capacity building and technology learning and therefore plays an important role during the transition period.

For the successful transition to the hydrogen economy, technologies capable of processing hythane efficiently are necessary. Solid Oxide Fuel Cells (SOFCs) are promising candidates due to their fuel flexibility, high efficiency, and a growing market [15]. The installed power and shipment of fuel cells increased from 516.5 MW and 63.2×10^3 units in 2016 to 2289.7 MW and 86.0×10^3 units in 2021. For SOFCs, specifically, 62.9 MW were installed, and 16.2×10^3 units were shipped in 2016, with deployment rising to 206.9 MW and 25.2×10^3 units in 2021. Data

E-mail address: r.styn@fz-juelich.de (R. Styn).

^{*} Corresponding author. Forschungszentrum Jülich GmbH, Institute of Energy Technologies (IET), Elektrochemische Verfahrenstechnik (IET-4), Wilhelm-Johnen-Straße, 52428, Jülich, Germany.

for 2016 are taken from "The Fuel Cell Industry Review" of 2021 [16] and 2022 [17]. The installed power is dominated by the transport sector, where powerful polymer electrolyte membrane fuel cell (PEMFC) are predominantly used in vehicles, while the number of shipped units is dominated by stationary fuel cells, as seen in applications such as micro-CHP systems in Japan. SOFCs are commonly used for stationary applications in buildings or data centers, with average power increasing from 3.9 kW in 2016 to 6 kW in 2020 [18]. The commercial segment of large-scale SOFC systems (200 kW to multiple MW) is expected to gain further importance due to its higher economic viability. The main contributors to market growth are North America, the Asia-Pacific region and Europe, which follow closely behind, while these systems are primarily deployed in the US, Japan, South Korea, and Europe. Between 2020 and 2023 the compound annual growth rate (CAGR) of the SOFC market were 9.6 % and is expected to be 11.5 % for the years 2023–2028 [19]. The SOFC market is predicted to grow the fastest compared to other fuel cell technologies [20].

The research and development activities of fuel cell manufacturers reflect the increasing interest in SOFC technology. The US-based company Bloom Energy installed 1 GW of cumulative system power in 2022. With their 330 kW 'Bloom Energy Servers', which are scalable to 10 MW, they account for 95 % of stationary fuel cell installations in the US since 2018 [21]. Robert Bosch GmbH has built and tested 100 kW systems in cooperation with Ceres Power, utilizing their metal-supported Ceres Power SteelCell[®] [22]. Several pilot projects are currently running, and in 2023 Bosch was granted € 160 million in funding by the German government to establish a production capacity of 200 MW/a [23]. In addition, Bosch and Ceres Power plan a strategic collaboration with Weichai Power for the Chinese market [24]. Convion Ltd. developed a stack together with Fraunhofer IKTS and Plansee SE [25] and produces 60 kW modules based on it [26]. FuelCell Energy offers 250 kW modules with electrical efficiencies of 62 % and 65 % for NG and H₂, respectively [27]. Research on pressurized hybrid plants has been conducted by LG Fuell Cell Systems [28] and Mitsubishi-Hitachi Heavy Industries. While LG's fuel cell division ceased operations in 2018 [29], Mitsubishi-Hitachi has installed 2.2 MW of their SOFC-GT system [30].

The key factor for the viable deployment of SOFCs is scaling up system power. Structural adjustments to electrode materials can enlarge the three-phase boundary and thereby enhance catalytic activity. Deseure et al. [31] demonstrated that the rate-determining step of the electrochemical reaction depends on the electrode structure, whereas Zhu et al. [32] investigated the advantages of ion-impregnated electrodes. However, enlarging the active cell area is challenging due to sealing problems or thermal stress, which can cause overheating, delamination, and microcracking, ultimately reducing the system's lifetime and efficiency [33]. A significant number of publications focus on connecting fuel cell stacks either in series or in parallel to reach high power levels. Araki et al. [34] modeled a low- and a high-temperature SOFC in series to enhance performance compared to two high-temperature SOFCs. Piroonlerkgul et al. [35] showed that connecting two stacks in series does not perform significantly better than a single stack. Improvements, however, could be obtained with a cooling unit between the stacks, which offers a wider operation range. In contrast, Kupecki et al. [36] showed that systems with two stacks in series perform better than systems with one stack module (two stacks in parallel) and a recirculation unit, achieving 3 to 7 %-points higher electrical efficiency. Additionally, Pirasaci [37] suggested connecting non-identical stacks in series, which resulted in higher electrical efficiencies compared to single and uniform multi-stack systems. To avoid disadvantages such as higher degradation of individual stacks in the serial configuration, parallel structures have been explored in several works. The power classes of SOFC systems range from small-scale applications [38] to the MW class [39]. Although mild operation conditions with minimized stress for the cells are achievable in parallel configuration [40], practical applications often suffer from maldistribution of fuel and air feeds, leading to non-uniform stack operation.

Optimized flow distribution within a single stack can improve performance by balancing temperature and voltage profiles [41]. On the system level, the distribution of flows among parallel stacks can influence transient behaviour [42] and the degradation of individual stacks [43]. By correlating these degradation patterns with operational inconsistencies, online detection and control strategies can be implemented in multi-stack systems [44]. A combination of serial and parallel structures can compensate the disadvantages of each connection strategy and provides a wide range of possibilities [45]. Marx et al. [46] showed for PEMFC that parallel structures result in less degradation, whereas Vivanpatarakij et al. [47] underlined for SOFCs the better performance of serial configurations due to higher voltages of the first stack. However, they did not model the pressure drop of the stacks and stated in a following study that the pressure drop significantly reduces electrical efficiency. Therefore, the stack design must be adapted for serial configurations to enhance performance [48]. Experimental investigations of Tomberg et al. [49] underlined the influence of practical design and the resulting maldistribution of the feed flow. The model-based study by Qin et al. [50] did not consider pressure drops along the fuel path and did not involve AEGR, which consequently led to results that differed from those in the aforementioned studies. This literature review showed that the main influence parameters for defining the best-performing stack configuration in multi-stack fuel cell systems are the fuel cell type, the process layout, and the resulting

Different experimental studies examine the influence of hydrogenblending on natural gas-based SOFC systems. Results indicate that the effects depend strongly on feed composition and reforming strategy. For example, methane addition to dry hydrogen can cause severe degradation of the cell if internal reforming is conducted without steam supply [51]. In contrast, the admixture of hydrogen to biogas-based systems with reforming unit positively affects degradation [52] and system performance [53], according to two studies from Panagi and his working group. Simic et al. [54] showed for a micro-CHP system that it can be operated under elevated hydrogen content in the feed maintaining safe operation, although the system adjustments by the manufacturer were not provided. Simulative studies focus on the impact of hydrogen-blending on the system performance and individual components. As shown by Cinti et al. [55], the operation with hythane of systems with internal reforming reduces thermal stress in the stack. With biohythane, the emission of biogenic CO2 is lowered, and the performance of the SOFC system is maintained [56]. The positive environmental effect of green hydrogen usage in fossil fuel based systems was also reported by Hai et al. [57]. As experimentally and simulatively also shown by Hormaza et al. [58], most studies support the feasibility of hydrogen blending in natural gas or biogas based systems, but the influence on the system performance varies in literature.

As the transition to sustainable energy systems requires innovative solutions that combine efficiency, scalability, and economic feasibility, this study addresses a critical gap in current research. It focuses on the effect of hydrogen-blending on SOFC performance, explores the opportunities offered by system upscaling, and evaluates the economic viability of large-scale SOFC systems adapted for hydrogen-blending, addressing the following key questions.

How does hydrogen-blending influence SOFC performance under defined operating conditions?

What cost reductions are achievable through the system scale-up? Are large-scale SOFC systems economically viable when adapted for hydrogen-blending?

By combining process simulation with techno-economic analysis, this study provides a holistic approach to understand the interplay between performance, cost, and scalability in SOFC systems. The novelty of the study lies in the detailed examination of the impact of hydrogenblending on system design and operation, as well as the integration of

economic considerations into the assessment of industrial-scale SOFC units. The findings not only highlight how hydrogen-blending impacts performance and how cost savings can be achieved through upscaling, but also confirm the economic feasibility of adapting SOFC systems to hydrogen-rich environments. These insights are relevant for accelerating the industrial adoption of the SOFC technology and contribute to achieving global decarbonization goals and implementing sustainable hydrogen as a central energy carrier.

2. Materials and methods

In the following, the selection and modelling of natural gas-based SOFC processes with steam reforming are presented and further, the upscaling strategy and the techno-economic analysis (TEA) method is explained. The process simulations were conducted in Aspen Plus and the TEA is based on an approach developed at the IET-4.

2.1. Process selection

SOFC processes mainly differ in the fuel treatment upstream or in the SOFC itself. Internal reforming reduces the component costs but causes thermal stress within the fuel cell due to the endothermic steam reforming reaction and the exothermic electro-chemical oxidation of the produced hydrogen. Therefore, the internal reforming leads to higher degradation and lifetime shortening. To overcome this issue, commonly external reformers are used in commercial and industrial applications. Possible reforming technologies are the catalytic partial oxidation (CPOX), steam reforming (SR) or autothermal reforming (ATR). The latter uses the generated heat from the partial oxidation for the steam reforming, so that external heating is reduced or unnecessary. The highest electrical efficiencies are reached with steam reforming systems [59], so that an SOFC process based on an external steam reformer is chosen to fit the scope of a cost competitive and reliable process. Besides, the desired hydrogen admixture could cause component damage in presence of oxygen during the CPOX and ATR reactions due to hot spot formation. For this reason, these reforming technologies are excluded.

The chosen process for the small-scaled system is shown in Fig. 1. The steam supply for the reformer is given by an anode exhaust gas recirculation (AEGR) to avoid a steam generator and enhance the electrical efficiency of the system.

According to Peters et al. [60], layouts with an adiabatic pre-reformer react less sensitive to high reactant utilization (RU) and recirculation ratio (RR), so that more flexibility is guaranteed for the hydrogen-blending. For this, two heat exchangers are necessary up-und

downstream of the reformer to heat up the fuel for the reforming reaction and to maintain the stack inlet temperature after the endothermic reforming. One part of the anode exhaust gas is combusted with the cathode air and used for the heating of the fuel gas and air. The other part is cooled down and recirculated for the steam supply. The important process design parameters are summarized in Table 1.

The upscaling of the process is based on the evaluation of industrial plants shown before. The target power of 240 kW is reached by a modular approach, in which stacks of a smaller power class are connected to realize the desired electrical output. In the same way, the scaled-up system can be adapted to the MW power class. In this study, four modulations of the stacks are investigated and shown in Fig. 2. They are named Ser1 - Ser4 after the number of modules, that the fuel gas passes one after the other in series. The focus is on the influence of the connection of the stacks and therefore, one reformer is implemented and the anode exhaust gas is recirculated upstream of the reformer. Different gas path configurations with AEGR of single stacks to different positions in the process are outside the scope of this study.

2.2. Modeling

The stack model is based on a commonly known approach applied in several studies dealing with process simulations in Aspen Plus [61]. It consists of different unit operations that are connected to simulate the electrochemical and reforming reactions within the stack, the oxygen ion transport through the solid electrolyte and the homogeneous temperature of the outlet streams. For a detailed description, the reader is

Table 1 Nominal process and design parameters for the small-scale (750 W) $\rm CH_{4}$ -fueled system shown in Fig. 1. Values represent the baseline simulation inputs used for model validation, including fuel composition, operating temperature, pressure, recirculation ratio, and reactant utilization.

System nominal power	750 W
Cell type	Electrolyte supported
Stack operation temperature	860 °C
Stack operation pressure	1 atm
Active cell area	128 A/cm ²
Cells per System	57
Stack current	18 A
Stack inlet temperature fuel/ air	680 °C
Stack outlet temperature fuel/air	860 °C
Efficiency of blower and pump	$\begin{array}{l} \text{Isentropic efficiency} = 76 \text{ \%, mechanical efficiency} \\ = 93.6 \text{ \%} \end{array}$

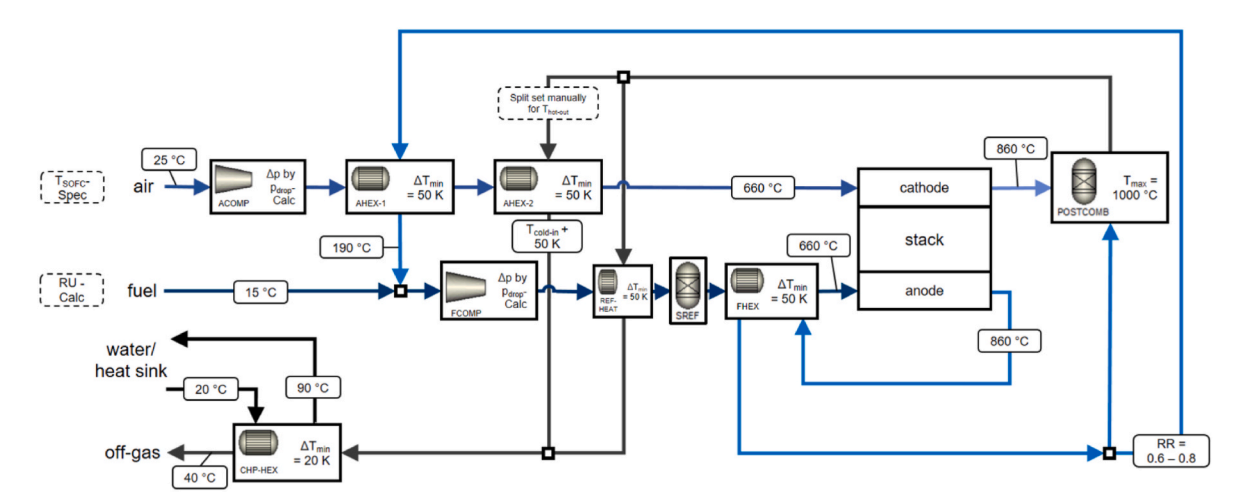


Fig. 1. Process flow scheme of the small-scale (750 W) CH₄-fueled system simulated in this study. The model includes fuel preheating, reforming, SOFC stack operation, afterburning of the anode off-gas, and heat recovery via a recuperative heat exchanger.

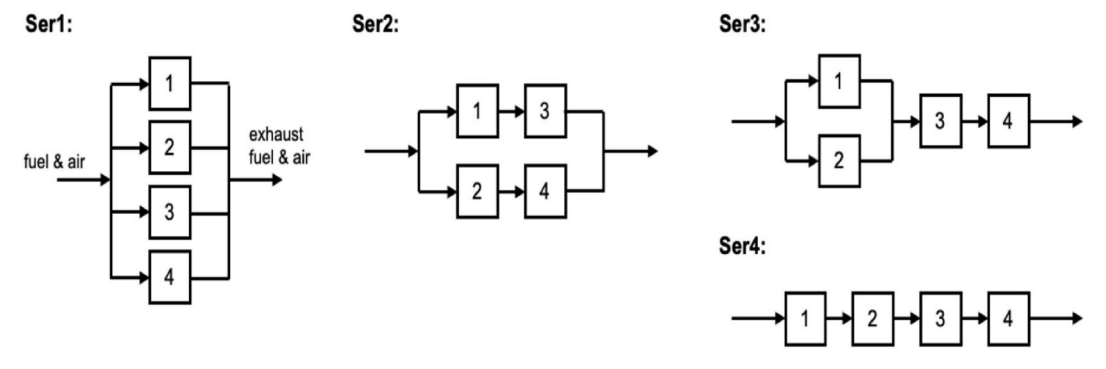


Fig. 2. Gas-path configurations (Ser1 to Ser4) for the upscaled SOFC (240 kW) systems evaluated in this study. Configurations differ in the arrangement of SOFC modules: Ser1–Ser4 represent increasing numbers of stacks connected in series per branch, while the number of parallel branches is adjusted to maintain total system output.

referred to the above-mentioned study.

The electrical output power of the single stacks is calculated with an electro-chemical model deposited in each stack model. The current drawn from the cell fueled with pure hydrogen is calculated with the Faraday's law according to equation (1).

$$I = z \cdot F \cdot \dot{n}_{H_2} \cdot RU \tag{1}$$

The stack voltage is calculated based on the Nernst voltage and polarization losses depending on the concentration in the anode and cathode channels and the stack temperature (equation (2)).

$$U(x_{i}, p, T) = U_{n}(x_{i}, p, T) - \eta_{oct}(x_{i}, p, T) - \eta_{ohm}(T) - \eta_{conc}(x_{i}, p, T)$$
(2)

The chosen SOFC stack is an electrolyte supported cell (ESC) with a 3 mol% yttria-stabilized zirconia (3YSZ) electrolyte, a Ni/CGO fuel electrode and an LSCF air electrode. The parametrization is based on the work of Leonide et al. [62] and Grosselindemann et al. [63] and adapted to the present case of this study.

The reforming reactions occurring in the stack and the reformer are steam reforming (equation (3)) and the water-gas-shift reaction (equation (4)).

Steam reforming
$$CH_4 + H_2O \rightleftharpoons CO + 3H_2$$
 $\Delta H = 206 \frac{kJ}{mol}$ (3)

Water – gas – shift
$$CO + H_2O \Rightarrow CO_2 + H_2 \Delta H = -41 \frac{kJ}{mol}$$
 (4)

The stack reactor and the reformer are modeled as equilibrium reactors so that no reaction kinetic approaches as suggested by Achenbach [64] and Aguir [65] for SOFCs are necessary in the steady-state process simulations.

The performance of the SOFC process is evaluated with the electrical and thermal efficiency as shown in Equations (5) and (6). These are defined as the electrical and thermal output divided by the energy input to the system. The electrical power $P_{el,net}$ is calculated from the electrical power drawn from the stack reduced by the power needed for the blower and pumps and losses of the DC/AC converter. The reference energy flow is calculated by the fuel mass flow multiplied by the lower heating value (LHV) of the fuel.

$$\eta_{\rm el} = \frac{P_{\rm el,net}}{\dot{m}_{\rm fuel,in} \cdot LHV_{\rm fuel,in}} \tag{5}$$

$$\eta_{\rm th} = \frac{\dot{Q}_{\rm sink}}{\dot{m}_{\rm fuel,in} \cdot LHV_{\rm fuel,in}} \tag{6}$$

To operate the stack in a reasonable and safe mode, the amount of converted hydrogen in the fuel cell is limited. For this, RU is defined as the share of hydrogen that is consumed by the electro-chemical reaction and the hydrogen supplied to the anode channel. Since the SOFC system is fueled with natural gas and the stack is composed of several cells,

equation (1) is adapted to calculate RU (equation (7)).

$$RU = \frac{I_{\text{stack}} \cdot N_{\text{cell}}}{F \cdot \dot{n}_{\text{an,in}} \cdot K_{\text{e}^-, \text{an,in}}}$$
(7)

Here, I_{stak} is the stack current, N_{cell} the number of cells, F the Faraday constant, $\dot{n}_{an,in}$ the molar flow rate of the gas at the anode inlet, and $K_{e\cdot,an,in}$ the average number of potentially releasable electrons per molecule of gas mixture at the anode. The latter one can be calculated by the following equation (8), specified for a methane fueled SOFC system [66].

$$K_{e^{-}} = \sum_{i} x_{i} \cdot N_{e^{-},i} = 8 \cdot x_{\text{CH}_{4}} + 2 \cdot x_{\text{CO}} + 2 \cdot x_{\text{H}_{2}}$$
 (8)

A too low RU results in inefficient operation and temperature peaks in the afterburner caused by the unreacted fuel. The lower limit depends on the desired performance, the used material and the overall process setup. Too high RU causes increased concentration polarization losses and irreversible damages of the anode through Ni oxidation. Consequently, an upper RU limit for this study is set to 0.8 as suggested by Schäfer et al. [66].

The AEGR above mentioned improves the system efficiency through a higher utilization of the fuel. The system reactant utilization (RU_{sys}) is similarly defined to the RU as the share of the fuel supplied to the whole system that is consumed by the electro-chemical reaction and can be calculated with RU and RR (equation (9)).

$$RU_{\text{sys}} = \frac{RU}{1 - RR \cdot (1 - RU)} \tag{9}$$

In reforming and SOFC processes, carbon deposition (CD), the formation of solid carbon on the reforming catalyst, the fuel electrode and in fuel supply lines and channels is possible. As consequence, increased pressure losses, electrical resistance and reduced active catalytic surfaces can be observed. CD is mainly driven by the reactions (10) to (12) [67].

Methane pyrolysis
$$CH_4 \rightleftharpoons 2H_2 + C \Delta H = 75 \frac{kJ}{mol}$$
 (10)

Boulouard equilibrium
$$2CO \rightleftharpoons CO_2 + C \Delta H = -173 \frac{kJ}{mol}$$
 (11)

Production of vapor CO + H₂
$$\rightleftharpoons$$
H₂O + C $\Delta H = -131 \frac{\text{kJ}}{\text{mol}}$ (12)

The risk of CD is reduced by high steam to carbon ratios (S/C) or the choice of the optimal reforming temperature. Too high S/C results in dilution of the feed and thus a voltage drop in the stack, whereas no optimal reforming temperature can favor the endothermal pyrolysis of methane at high temperatures or the exothermal Boudouard reaction and vapor production at low temperatures. Therefore, the risk of CD must be observed especially at the outlet of the reformer and the stack

[66]. For this, two approaches are introduced based on the reaction equilibria and the reaction kinetics. First, an equilibrium condition is formulated to examine whether CD is thermodynamically possible (equation (13)–(15)). The equilibrium constants $K_{c,i}$ [68] depend on the temperature and are compared to the reaction quotient $Q_{c,i}$. The formation of carbon is possible if $\alpha_i > 1$.

$$\alpha_{\text{pyrolysis}} = K_{c,\text{pyrolysis}} \cdot \frac{p_{\text{CH}_4}}{p_{\text{H}_2}^2} = K_{c,\text{pyrolysis}} / Q_{c,\text{pyrolysis}}$$
(13)

$$\alpha_{\text{boudouard}} = K_{c,\text{boudouard}} \cdot \frac{p_{\text{co}^2}}{p_{\text{co}_2}} = K_{c,\text{boudouard}} / Q_{c,\text{boudouard}}$$
(14)

$$\alpha_{\text{vapor}} = K_{c,\text{vapor}} \cdot \frac{p_{\text{CO}} \cdot p_{\text{H}_2}}{p_{\text{H}_2}} = K_{c,\text{vapor}} / Q_{c,\text{vapor}}$$
(15)

The reversibility of the reactions implies that the equilibrium criterion alone is insufficient to describe the CD potential. As mentioned above, temperature affects the formation of carbon differently for the three reactions. Therefore, the reaction kinetic scheme proposed by Snider et al. [69], shown in equations (16)–(21) (see Table 2), was implemented. This approach accounts for the formation or depletion rate of solid carbon by considering the overlapping effects of the reactions. The rate equations were formulated for coal gasification, so the parameter $m_{\rm s}$ (mass of solid carbon) is chosen arbitrarily. Nevertheless, the combined rate expressions provide qualitative insights into the formation or depletion of carbon.

In a multi-stack SOFC system with AEGR and varying gas path configurations, pressure losses (p_{loss}) significantly affect system performance. For this reason, the p_{loss} of individual stacks was described by volume flow-dependent correlations. A linear approach was applied for the cathode side, while a quadratic approach was chosen for the anode side. To account for the total pressure loss in the system, additional p_{loss} contributions from relevant balance of plant (BoP) components were included in the calculations. Based on simulations by van Biert et al., in 2020 [70], these included a loss of 0.02 bar for each passage through the reformer, post-combustor, or one of the heat exchangers.

The summed pressure losses for the air and fuel paths were factored

Table 2Reaction rate equations for the carbon-deposition mechanisms considered in this study, including methane pyrolysis, the Boudouard reaction, and CO reduction.

Reaction		Rate expression $\frac{\text{mol}}{\text{m}^3 \cdot \text{s}}$	
		m ³ ·s	
	ane pyrolysis	(10.570	(10)
fw	$CH_4 \rightarrow 2H_2 + C$	$r_{\text{pyrolysis,f}} = 2.0.151 \cdot m_{\text{s}} \cdot T^{0.5} \cdot \exp\left(\frac{-13,578}{T}\right)$	(16)
		0.372) \cdot [CH ₄] ^{0.5}	
bw	$2H_2 + \ C \rightarrow CH_4$	$r_{\text{pyrolysis,b}} = 2 \cdot 1.368 \cdot 10^{-3} \cdot m_{\text{s}} \cdot T \cdot \exp\left(\frac{-8,078}{T}\right)$	(17)
		7.087)·[H ₂]	
Boud	louard Equilibrium	,	
fw	$2CO \rightarrow CO_2 + C$	$r_{\text{boudouard,f}} = 1.044 \cdot 10^{-4} \cdot m_{\text{s}} \cdot T^2 \cdot \exp\left(\frac{-2,363}{T}\right)$	(18)
		$(20.92) \cdot [CO]^2$	
bw	$CO_2 + C \rightarrow 2CO$	$r_{\text{boudouard,b}} = 1.272 \cdot m_{\text{s}} \cdot T \cdot \exp\left(\frac{-22,645}{T}\right) \cdot [\text{CO}_2]$	(19)
coı	uction and nsumption of por	,	
fw fw	$CO + H_2 \rightarrow$	(-6,319	(20)
	$H_2O + C$	$r_{\text{vapor,f}} = 1.044 \cdot 10^{-4} \cdot m_{\text{s}} \cdot T^2 \cdot \exp\left(\frac{-6,319}{T}\right)$	
		17.29)·[H ₂]·[CO]	
bw	$\begin{array}{cc} H_2O + C \rightarrow H_2 + \\ CO \end{array}$	$r_{\text{vapor,b}} = 1.272 \cdot m_{\text{s}} \cdot T \cdot \exp\left(\frac{-22,645}{T}\right) \cdot [\text{H}_2\text{O}]$	(21)

^{*} fw, forward; bw, backward.

into the blowers' power calculation as their set pressure increase. The consumed air and fuel were assumed to enter the post-combustor at the same pressure level, while the cold off-gas exited the system at atmospheric pressure. The blowers impacted the system efficiency through their power consumption, reducing the net power output. Their isentropic and mechanical efficiency were set to 0.76 and 0.936, respectively.

2.3. Techno-economic assessment

The effects of upscaling and the cost competitiveness of SOFC systems adapted for the hydrogen-blending are evaluated with the technoeconomic analysis. Since the TEA is developed for large-scale chemical plants, the approach is adapted for the evaluation of the SOFC systems. First, the original procedure is presented and thereafter the adaptations to the SOFC systems are explained.

The specific costs per kWh electricity, also referred to as cost of manufacturing (COM), were obtained based on the annual capital costs (ACC) and the operational expenditures (OPEX). Since the costs commonly are given on an annual basis, the capital expenditures (CAPEX) were adapted to the operation time considering interest rate and the loss of value of the working capital, summarized in the annual capital costs. CAPEX and ACC were calculated with the investment costs (FCI), the dependencies are shown in equations (22) and (24).

$$COM = ACC + OPEX (22)$$

$$ACC = FCI \cdot \left(\frac{i \cdot (1+i)^t}{(1+i)^t - 1} + 0.15 \cdot i \right)$$
 (23)

$$CAPEX = 1.15 \cdot FCI \tag{24}$$

To determine the investment costs, in a first step, the component costs C_0^0 were calculated based on the methodology suggested by Turton [71], see equation (25). K_1 , K_2 and K_3 are empirical parameters and A is the capacity or size parameter. For calculation of C_0^0 for components, whose size is under the lower validity limit, a degression coefficient d was introduced (equation (26)). With a valid pair of values for A, this coefficient was calculated according to equation (27). The data set of Turton is valid for the year 2001, therefore the current costs considering the inflation were calculated with equation (28) and the chemical engineering plant index (CEPCI).

$$\log_{10}\left(C_{\rm p}^{0}\right) = K_{1} + K_{2} \cdot \log_{10}(A) + K_{3} \cdot \left[\log_{10}A\right]^{2} \tag{25}$$

$$C_{\rm p}^0 = C_{{\rm p}A_{\rm min}}^0 \cdot \left(\frac{A}{A_{\rm min}}\right)^d \tag{26}$$

$$d = \frac{\ln(c_{\rm pl}^{0}/c_{\rm p2}^{0})}{\ln(A_{1}/A_{2})} \tag{27}$$

$$C_{p,2024}^{0} = C_{p,2001}^{0} \cdot \frac{CEPCI_{2024}}{CEPCI_{2001}}$$
(28)

The investment costs were calculated with the component costs considering installation costs by the parameters B_1 , B_2 , F_m and F_p (Equation (29)) and a share of 0.5 of the component costs for other investments like storages or side plants (Equation (30)).

$$C_{\rm BM} = C_{\rm P}^0 \cdot (B_1 + B_2 \cdot F_{\rm M} \cdot F_{\rm P}) \tag{29}$$

$$FCI = 1.18 \cdot \sum_{i=1}^{n} C_{BM} + 0.5 \cdot \sum_{i=1}^{n} C_{P}^{0}$$
(30)

The OPEX sum up costs for raw materials, utilities, operating laboratory, waste treatment, and several others (that were determined with surcharge factors by Turton). Raw material and utility costs resulted

from multiplication of their consumption in the process and their specific cost. For a detailed description of the OPEX determination, see the above-mentioned work of Turton.

The presented methodology is developed for large-scaled chemical plants. In this study, the cost calculation was adapted in such a way that the power class, production capacity of the SOFC systems and their commercialization are considered. Therefore, the cost for engineering and shipment, which are included in the investment cost, were neglected. To calculate the component cost, the data published in a detailed manufacturing cost assessment by the Battelle Memorial Institute were used for small-scale [72] and large-scale systems [73]. The manufacturing costs were adapted to the systems size by the factor f_{size}, which is linear to the system size scaling (0.75 for transfer from 1 kW to 750 W system and 0.96 from 250 kW to 240 kW system). The costs for blowers and heat exchangers were obtained with the presented methodology, because of the different system layout and heat management compared to that evaluated by Battelle. The increased production quantity was considered through the factor f_{production} by a linear correlation of the cost decrease for blowers and heat exchanger in the assessment of Battelle. Since SOFC systems are sold in high quantities, the costs for engineering, installation and other aspects were summarized in a sales markup and assembly costs for the whole system, according to Battelle. Therefore, equations (29) and (30) were not considered to calculate the investment costs.

The operational expenditures (OPEX) in this study include fuel costs and annual maintenance costs according to the method of Turton as 6 % of the FCI per year. This covers scheduled servicing, component replacement, and system inspections. The prices for the fuels (natural gas and hydrogen) depend on the purchase quantity and are listed Table 3. For the small-scale system simulation household prices were taken and the large-scale system were treated as industrial end user. The hydrogen price used in this study was derived from the "Hydex" index published by E-Bridge Consulting [74], which represent a future-oriented cost benchmark for hydrogen production in Germany. This index intends to support investment decisions and reflect projected market conditions rather than current spot prices. The selected value therefore represents an optimistic but industry-backed scenario, consistent with the long-term perspective of the techno-economic analysis.

For calculating the electrical power in an alternating current (AC) net, an inverter efficiency of 0.95 was used. Additionally, a comparison was carried out with the case that the thermal energy supplied by the system is used. Here, the amount of heat offered was calculated back to the NG costs, a heater with a thermal efficiency of 0.98 would need to provide the same amount of heat. The underlying assumption is that the produced heat can be used.

3. Results and discussion

Based on the above-mentioned modeling and boundary conditions, different parameter studies were carried out as shown in Table 4. The parameters RR and RU were varied from 0.6 to 0.8 and 0.5 to 0.75. Values for RR above 0.8 were not considered in this study, as the system's thermal integration reached its practical limits in this range. The

Table 3 Natural-gas (NG) [75] and hydrogen (H_2) prices [74] as a function of purchase quantity and end-user type. Prices are given in ϵ /MWh for the reference year [2024] and are based on European market data. Households are marked with "h", industrial end users with "non-h".

Fuel	Purchase quantity range	Price in €/kWh
NG	h, <5600 kWh	140.5
NG	h, 5600–55600 kWh	114.5
NG	non-h, 278-2778 MWh	95.2
NG	non-h, 2778-27778 MWh	80.5
H_2	_	89.81

Table 4Simulation cases considered in this study: small-scale (750 W) SOFC with NG (E1) and elevated H₂ content (E2), large-scale (240 kW) SOFC with gas-path configurations Ser1 – Ser4 (E3) and H₂ parameter study based on Ser1 (E4).

No.	System size/name Short description	Parameter (range, step size)	Objective
E1	750 W NG parameter study	RR (0.6–0.8, 0.05) RU (0.5–0.75, 0.05)	Choose best feasible parameter set for $\eta_{\rm el}$
E2	750 W H ₂ -share parameter study	RR (0.7–0.8, 0.05) RU (0.6–0.75, 0.05) $\Phi_{\rm H2}$ (0–0.3, 0.1)	Check feasibility of H_2 admixture and effect on $\eta_{\rm el}$
E3	240 kW – Ser1 – Ser4 Gas path configuration and NG parameter study	RR (0.7–0.8, 0.05) RU (0.6–0.75, 0.05)	Choose best layout in terms of $\eta_{\rm el}$
E4	240 kW – Ser1 H ₂ -share parameter study	RR (0.7–0.8, 0.05) RU (0.6–0.75, 0.05) $\Phi_{\rm H2}$ (0–0.3, 0.1)	Check feasibility of H_2 admixture and effect on η_{el}

heat exchanger would either become prohibitively large and costly, or the maximum transferable heat could not be practically achieved. 0.75 for RU is the higher limit to avoid fuel depletion in the stack. The fuel cell is operated in galvanostatic operation mode and the feed stream is adapted to reach the target value of RU. The aim of the simulations was to evaluate the influence of hydrogen admixture on the SOFC process and figure out the impact of the gas path configuration on the system performance.

3.1. Model validation

To validate the electrochemical model, simulation results were compared with experimental data for a commercial Sunfire cell as reported by Riegraf et al. [76]. The cell used in the experiments features a 3YSZ electrolyte (90 μm), Ni/CGO fuel electrode (20 μm), and an LSCF air electrode (25 μm). The cell was operated with a fuel mixture of 97 % H_2 and 3 % H_2O and air, each with a flow rate of 1 l/min at an operating temperature of 860 °C.

Fig. 3 shows calculated and experimental polarization and power density curves, with experimental data represented by symbols and simulation results by solid lines. The simulated polarization curve aligns well with the measured cell voltage. The largest deviation is observed at open-circuit conditions, with an absolute error of 0.0267 V (2.49 %). The power density curve also shows good agreement with the experimental data. At higher current densities, voltage deviations become more pronounced, leading to a maximum power density error of 0.01316 W cm $^{-2}$. The standard deviations of 0.01257 V and 0.00559 W cm $^{-2}$ confirm the validity of the model across the relevant current density range.

3.2. Small-scale results

Fig. 4 shows the influence of RR on the direct current electrical efficiency at varying RU. The achieved efficiencies reach from 54.8 % to 65.6 % while keeping the values for RR and RU in the mentioned limits (Table 4). For constant fuel consumption in the stack up to RU = 0.70, the electrical efficiency increases with higher recirculation of the anode exhaust gas due to higher RU $_{\rm sys}$. At a RU higher than 0.70, an optimum of the electrical efficiency can be observed. On the one hand, high RR and RU lead to a dilution of the anode feed gas which lowers the cell voltage and therefore the electrical power output. On the other hand, the increased power consumption of the blower at high RR diminishes the electrical net power and therefore the efficiency. With this, the findings

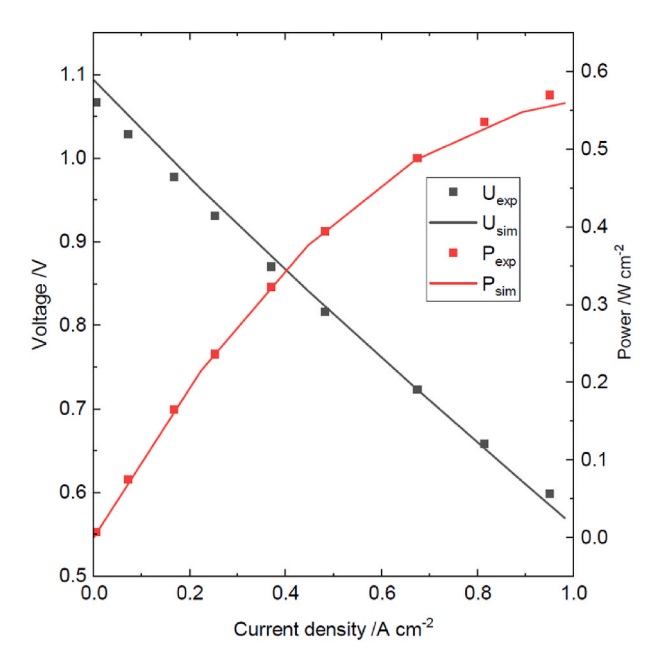


Fig. 3. Polarization and power density curve based on the electrochemical model embedded in the fuel cell model. Operating conditions (860 $^{\circ}$ C, fuel mixture of 97 $^{\circ}$ H $_2$ and 3 $^{\circ}$ H $_2$ O, 1 l/min flow rate on both anode and cathode sides) and experimental data a taken from Ref. [76]. Experimental data (exp) represented by symbols and calculated data (sim) by solid lines.

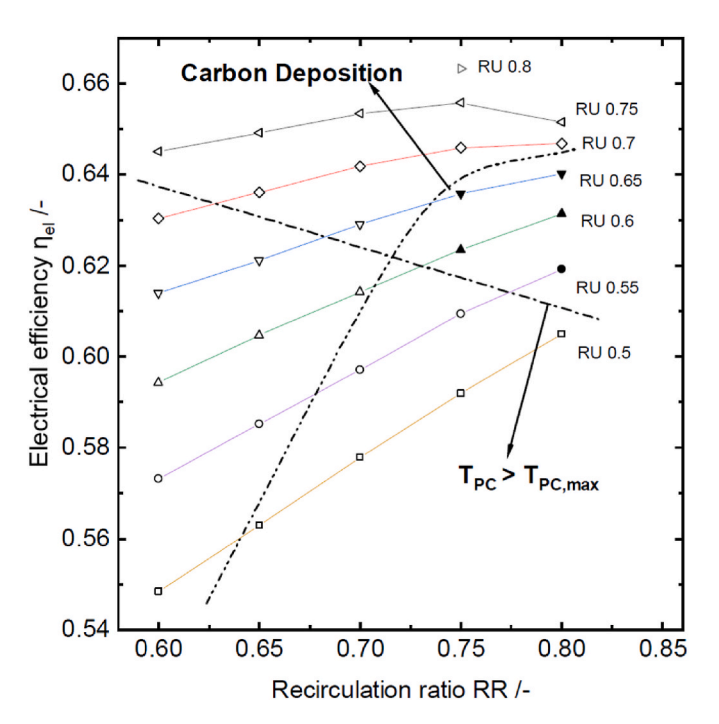


Fig. 4. Electrical efficiency as function of RR. Dash-dotted lines indicate limits for carbon deposition and post-combustor temperature, while filled symbols represent feasible operating configurations.

of Peters et al. [60] could be reproduced, thereby verifying the validity of the overall process model. Similar dependencies of RU and RR have also been observed in the operation of more integrated systems, as reported by Engelbracht et al. [77]. Compared to the less complicated system in the study by Hollmann et al. [38], the present configuration is 9.4 % more efficient. Higher efficiencies were expected but the results indicate that the zero-dimensional resolution and idealised assumptions lead to overestimated efficiencies. However, the operation of SOFC

systems can be reproduced, and comparisons between different use cases remain valid.

The operation is limited by two criteria as shown in Fig. 4. The dashdotted-lines show the restriction for the post-combustor (PC) temperature and the carbon deposition. For low RU, the fuel is not electrochemically consumed in the stack and therefore burned in the postcombustor that causes temperatures above 1000 °C. The simulations show that a minimal RUsys of 0.855 is necessary to prevent too high temperatures in the afterburner. Regarding the carbon deposition, low RR and high RU lead to a lower H2 and a higher CH4 concentration at the stack inlet. At a stack inlet temperature of 660 °C these conditions favor methane pyrolysis. Therefore, high RR and low RU are suggested to reach high RUsys and consequently high electrical efficiencies at safe operation conditions. The resulting feasible parameter sets are shown in Fig. 4 by the filled symbols in the area between the curve for the CD and temperature limits. From 30 investigated operation points, five parameter sets are suitable, thus the operational range is strongly influenced by the carbon deposition and PC temperature. The highest electrical efficiency of 64.0 % is achieved with a RR of 0.8 and a RU of 0.65.

Fig. 5 shows the impact of hydrogen-blending on the SOFC system performance. The fuel input is controlled to realize RRs between 0.7 and 0.8 and RUs between 0.6 and 0.8. Further operation points are not considered because of lower electrical efficiencies achieved. For constant RR-RU sets, a decrease in electrical efficiency of up to 1.5 % point for 30 vol% $\rm H_2$ is observed. The negative influence of hydrogen blending on the system performance as also shown by Hormaza et al. [58], is caused by two different effects. On the one hand, the volume flow increases and therefore also the power consumption of the fuel blower at higher hydrogen content in the feed. According to equations (7) and (8) the needed molar feed flow for constant RUsys can be calculated by equation (31) with the molar flow rate of hythane $\dot{n}_{hyth,f}$ and methane $\dot{n}_{CH_4,f}$ and the hydrogen share in the feed $x_{H_2,f}$.

$$\dot{n}_{\rm hyth,f} = \frac{4}{4 - 3 \cdot x_{\rm Ho,f}} \dot{n}_{\rm CH_4,f} \tag{31}$$

On the other hand, the higher energy input at elevated hydrogen content in the feed reduces the electrical efficiency causing 90 % of the decrease. The energy input at constant RU_{sys} and varying molar hydrogen share is calculated with equation (32), using the fuels' lower heating value ratio $K_{LHV}=\frac{LHV_{mol,H_2}}{LHV_{mol,CH_4}}.$ Inserting the lower heating values of hydrogen (241.84 kJ/mol) and methane (802.35 kJ/mol), equation (32) shows that the energy input using a hythane feed is higher than that of a pure methane feed. Therefore, no adaptation of the fuel feed leads to higher efficiencies at elevated hydrogen content but also causes more stress for the fuel cell [55].

$$\dot{n}_{\text{hyth,f}} \cdot LHV_{\text{mol,hyth}} = \frac{4 - 4 \cdot x_{\text{H}_2,\text{f}} \cdot (1 - K_{\text{LHV}})}{4 - 3 \cdot x_{\text{U.f}}} \cdot \dot{n}_{\text{CH}_4,\text{f}} \cdot LHV_{\text{mol,CH}_4}$$
(32)

Against the reduction of the electrical efficiency at constant RR and RU, less potential of CD as effect of H_2 admixture enhances the possible system performance. Because of less carbon supplied to the system, the problem of carbon deposition (CD) at the stack inlet is reduced, as also shown by Panagi et al. [52] for a biogas fed system. Thereby, new parameter sets with higher η_{el} become feasible, which fully outplays the efficiency reduction mentioned before. As shown in Fig. 5, the marked operation points are possible because of the positive effect of hydrogen-blending. For 30 vol% H_2 , a parameter set with RU =0.8 even becomes feasible.

While hydrogen blending offers clear benefits in terms of carbon suppression, it also introduces engineering challenges. Higher hydrogen content increases volumetric flow rates, as discussed above (Equation (32)), and therefore requires adapted blower sizing and control. In addition, hydrogen's thermal properties can alter the stack's temperature distribution, an effect that cannot be captured with the zero-dimensional approach used in this study. Material-related issues

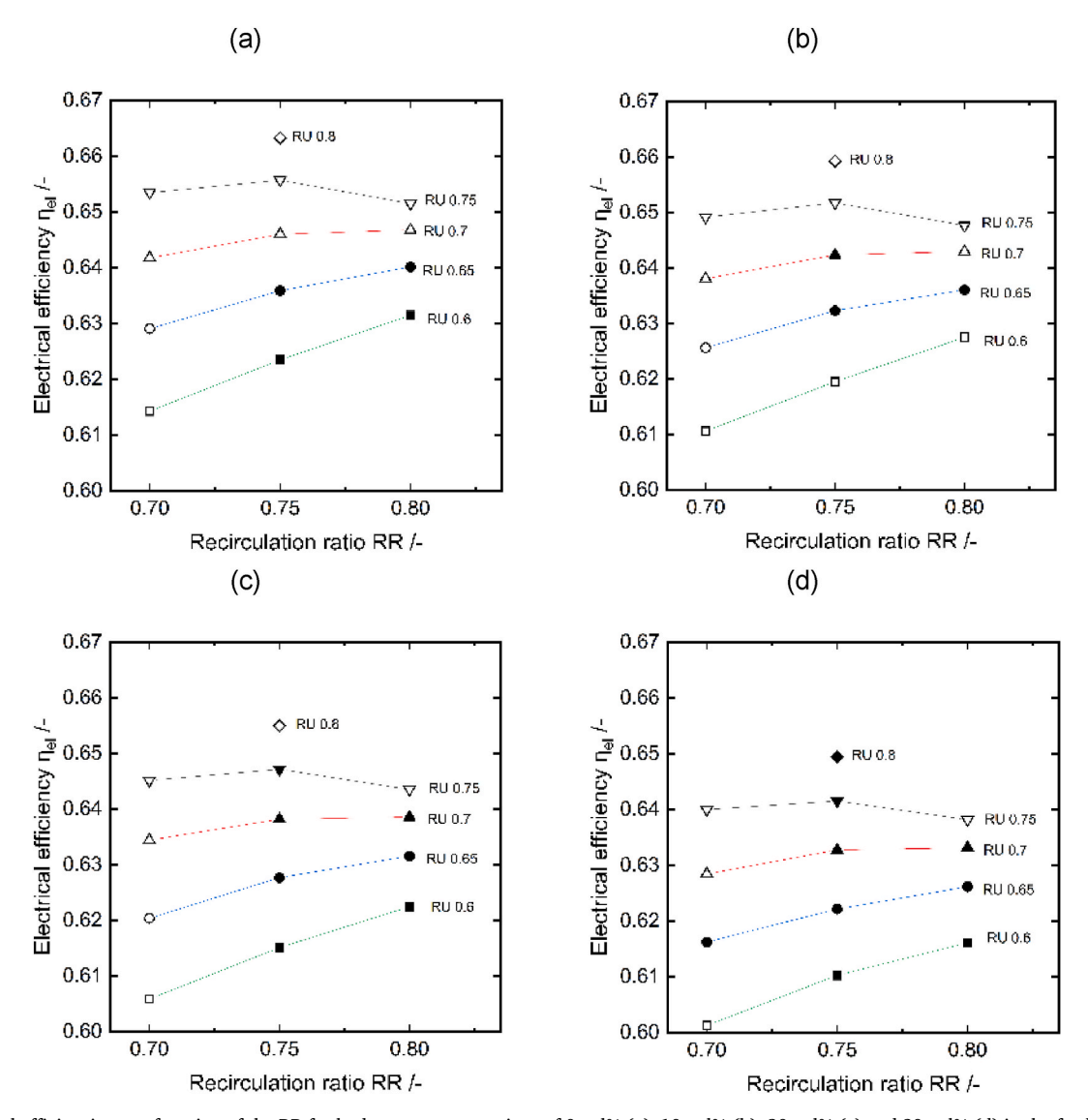


Fig. 5. Electrical efficiencies as a function of the RR for hydrogen concentrations of 0 vol% (a), 10 vol% (b), 20 vol% (c) and 30 vol% (d) in the feed. Filled symbols represent feasible operating configurations, considering carbon deposition and post-combustor temperature limits.

include increased gas permeability through seals and potential hydrogen embrittlement of metallic components. These aspects should be addressed in future studies.

3.3. Large-scale results

In the following section, the upscaling of the system and the gas path configuration is investigated. The simulation results of the multi-stack systems for natural gas, as described in section 2.1, are shown in Fig. 6. The dependency of the electrical efficiency on RU and RR strongly differs for the different gas path configurations and consequently also from the single stack system. The highest efficiencies are reached by the parallel structure (Fig. 6 a) with a RR of 0.8 and a RU of 0.65. Fig. 6 c and d show that with more stacks connected in series, higher RU at constant RR is feasible, but does not make those systems reach the higher efficiencies of the systems with more parallelization (Fig. 6a and b). The efficiency decrease of the serial configuration is 6.0 % points, hence significantly lower compared to the parallel structure.

This behavior results from the system's pressure loss and the temperature distribution along the gas path. For the parallel structure, the volume flows of fuel and air are distributed on the entire number of single cells in the system. In contrast, the volume flows in the system

with four stacks in a row are the same for each stack. Therefore, the pressure losses are higher due to the higher volume flow per cell and sum up due to the serial connection. The fuel and air blower energy demands are higher and lower in consequence the electrical efficiency of the system. This observation is in line with experimental studies by Assabumrungrat et al. [48] and shows the unavoidable need to consider the increased losses for the large-scale systems. Additionally, the RU for each stack in the serial structure is lower than in the parallel structure und thus, less heat is released by the electrochemical reaction. The averaged temperature of each stack differs along the gas path, as shown in Fig. 7. The low temperature in the front modules causes high ohmic losses which leads to lower cell voltages and lower electrical power. To enhance the performance of serial structured systems, the anode and cathode flow channels must be modified to achieve lower pressure losses [48] and the stacks can be operated at different currents to adapt the stack temperatures [36]. Without these modifications, a parallel stack configuration is suggested with a RR of 0.8 and a RU of 0.65.

The hydrogen-blending effects the large-scale system's behavior in the parallel configuration in the same way as that of the small-scale system, as consequence of the design approach. Four stacks in parallel can be seen as one large stack, therefore the results for the small-scale system are transferable to the large-scale parallel system and not

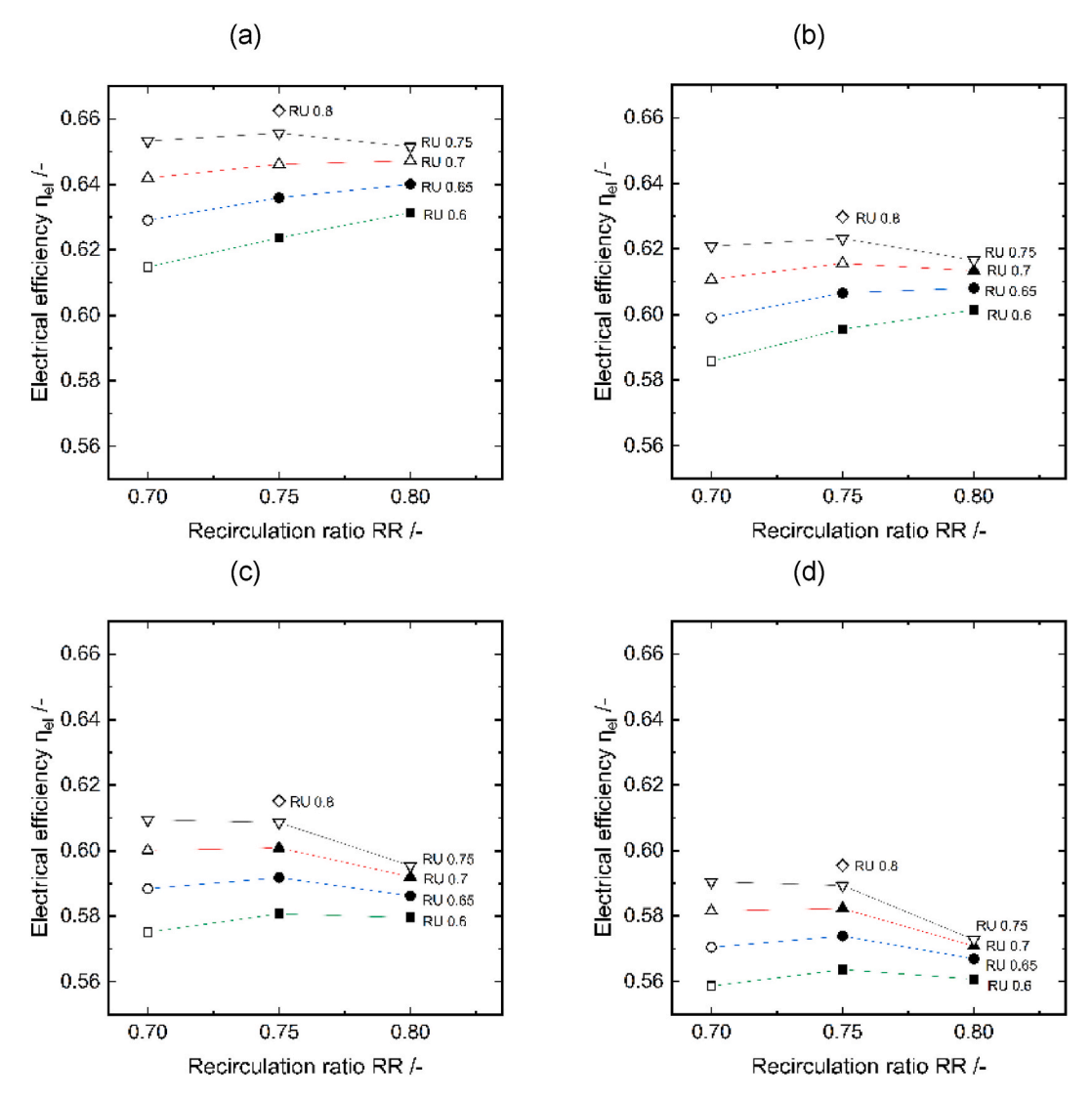


Fig. 6. Electrical efficiency as a function of the recirculation ratio (RR) for large-scale (240 kW) systems with gas-path configurations Ser1 (a), Ser2 (b), Ser3 (c), and Ser4 (d), all fueled with natural-gas. Filled symbols represent feasible operating configurations that satisfy both carbon-deposition limit and the post-combustor temperature constraint.

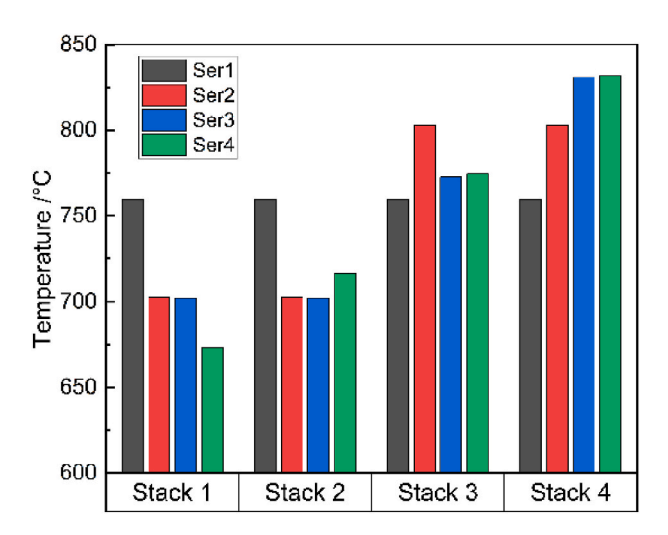


Fig. 7. Averaged stack temperature for large-scale (240 kW) SOFC systems with the gas-path configurations Ser1 – Ser4, fueled with natural-gas.

shown here. Additionally, the disadvantages of more serial system layouts should also be observed at higher hydrogen concentrations in the feed. According to equation (31) the molar hythane flow increases with higher hydrogen content in the feed, so that the pressure losses and the blower power consumption diminish the electrical efficiency even more. It is assumed that the wider operation range as consequence of less carbon deposition at elevated hydrogen share in the feed does not compensate the high losses of serial stack configurations. Therefore, the parallel configuration is also suggested for the hydrogen-blending in the large-scale system.

3.4. Results of techno-economic assessment

Since the economic viability is predominantly determined by the electrical efficiency, for the techno-economic analysis, the best performing systems regarding η_{el} from the technical assessment are chosen. To evaluate the influence of the scale up and the hydrogen admixture on the COM, the natural gas fueled small-scale system, the NG-based scaled up system in parallel structure and a large-scale system in parallel structure adapted to hythane fuel is analyzed. Latter is dimensioned to an operation under elevated hydrogen content without replacement of blowers and heat exchangers for different hydrogen contents in the fuel.

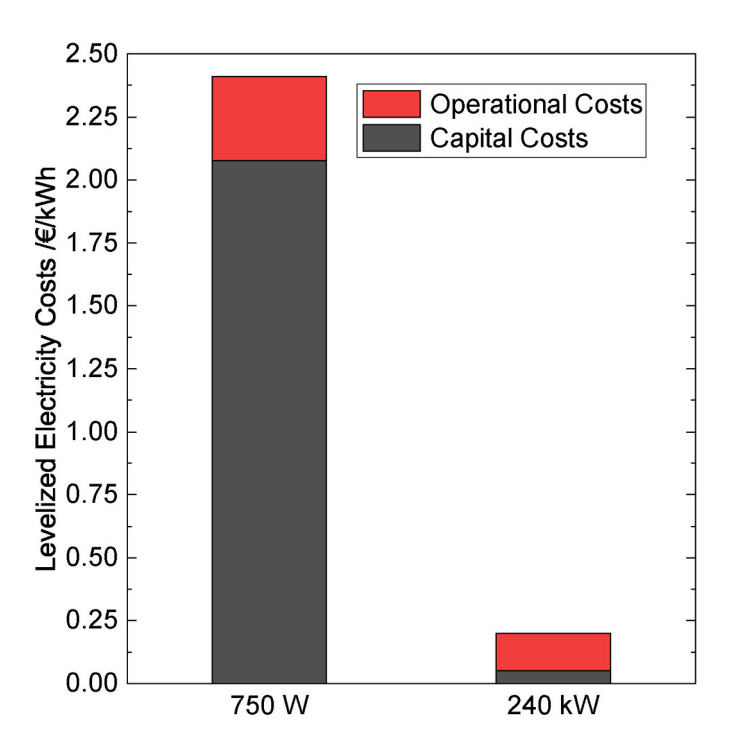


Fig. 8. Levelized electricity cost (ε /kWh) divided in capital and operational cost for the small-scale (750 W) and large-scale (240 kW) system fueled with natural gas.

The used parameter sets (RR, RU) for the calculation of the operational cost of the small- and large-scale system fueled with NG are (0.8, 0.65) and for the large-scale system fueled with hythane are (0.8, 0.65) for 0 % $\rm H_2$, (0.75, 0.7) for 10 vol% $\rm H_2$, (0.75, 0.75) for 20 vol% $\rm H_2$, and (0.75, 0.75) for 30 vol% $\rm H_2$. The latter does not use RU = 0.8, although previous simulations indicated feasibility with this value, due to increased caution against fuel depletion. The systems are included in the overview in Table 4.

Fig. 8 shows the costs per kWh divided into capital and operational costs for the 750 W and the 240 kW system fueled with natural gas. The annual capital costs are calculated with an interest of 8 % and the annual electricity production results from an operational time of 6000 h per year. The costs per kWh electrical energy supplied by the small-scale systems with 2.41 ϵ /kWh are by a factor of twelve higher than these of the scaled-up system with 0.20 ϵ /kWh. The corresponding costs of

electrical energy on the market are 0.4 €/kWh and 0.18 €/kWh for the electricity production capacity of the small- and large-scale system [78]. Accordingly, the small-scale system cannot compete with the market prices and should not be manufactured. Against that, the large-scale system offers the opportunity to generate decentralized electrical power with comparable costs. The highest amount of costs for the 750 W system results from the capital costs. The operational costs only contribute with 14 % to the total costs for this system, whereas the capital costs are mainly driven by the BoP, especially the heat recovery system which contributes with a share of 93 % to the overall capital costs. Hence, the heat recovery system with the highest total share of costs has the most potential for cost reduction in this case. In contrast, the large-scale system costs are mainly driven by the operational costs. These are given by the market, therefore the cost reduction potential of large-scale system is lower compared to the small-scale system. The CAPEX for the large-scale SOFC system operated with natural gas (2684 €/kW) are in good agreement with the cost analyses of the "Fuel Cells and Hydrogen Joint Undertaking" that stated costs up to 4024 €/kW [79]. Calculated costs for these systems strongly depend on the process layout, because of the high share of the BoP and therefore comparison should be made carefully. With this amount of uncertainty, the costs of this study are considered as viable.

As mentioned before, the system for hydrogen-blending is designed to process natural gas with different shares of hydrogen up to 30 vol%. The comparison of the energy costs is shown in Fig. 9 (a). The system adaption results in an increase of 0.0006 ϵ/kWh for the operation under pure methane. The changes of the BoP, especially larger heat exchangers, increase the capital costs of the adapted system fed with pure methane (H00). With higher H_2 content in the feed, the efficiency gain due to the wider operational range conquers with the higher feed flow of hythane compared to methane and the fuel costs. Additionally, the different energy output per year diminishes the impact of the capital costs for the compared systems. These effects result in decreased energy costs for 10 vol% H_2 compared to the NG operation of the adapted system and slightly higher energy costs for 20 and 30 vol% H_2 . The adapted balance of plant increases the cost per kWh electrical energy by maximal 0.0033 ϵ , hence related to the natural gas system by 1.6 %.

To take future policies and evolutions of the energy market into account, the payback time (PBT) for the different systems were calculated based on the assumption of the investment in a SOFC plant and the sale of electricity. Fig. 9 (b) illustrates the PBT for the 240 kW system variants under varying electricity prices. The calculation assumes 6000 operating hours per year and a 20-year lifetime. As shown, the systems become economically viable (PBT <20 years) at electricity prices of approximately 0.23 ϵ /kWh or higher. The PBT for a given electricity

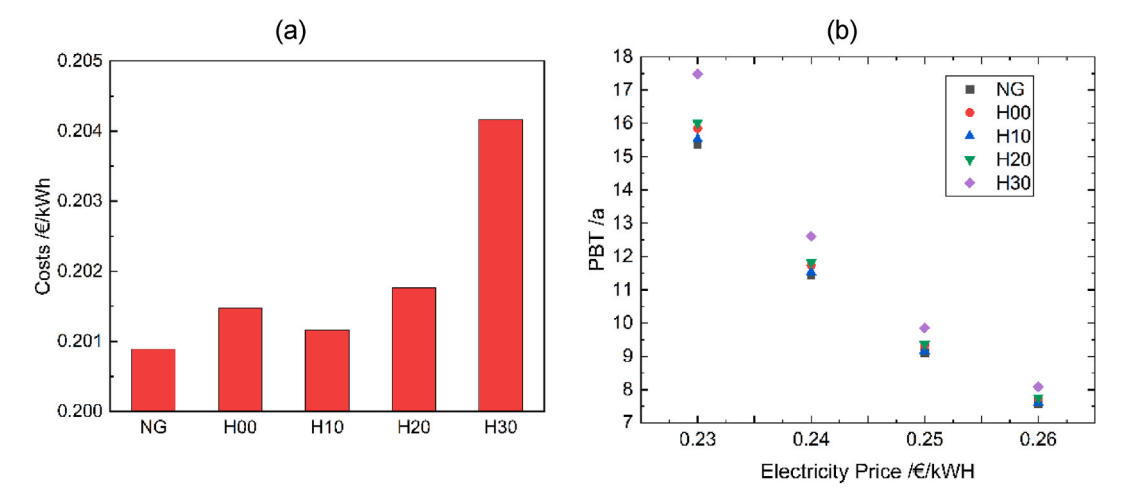


Fig. 9. (a): Costs per kWh for the large-scale systems considered in this study. H00 – H30 represent the hydrogen content in the fuel (0–30 vol%). (b): PBT of the Systems (H00 – H30) depending on the electricity price.

price increases with the hydrogen content as consequence of higher capital and operational expenditure. The results highlight that investment recovery is more sensitive to market conditions than the choice of fuel and reasonable PBT can be reached for realistic electricity prices.

The TEA carried out is based on the simulation described in sections 3.1 and 3.2. Therefore, the economically viable and safe operation under elevated hydrogen content in the feed is technically possible and should be considered to address possible changes in the natural gas supply net. Nevertheless, several engineering challenges remain outside the model scope. These include thermal management between stacks, uniform gas distribution, and start-up/shutdown control. In large systems, local temperature and flow imbalances can impact performance and durability that effects the economic viability of the technology. Addressing these aspects requires detailed modelling with higher resolution and experimental validation in future studies.

4. Conclusions

This study investigated the effect of hydrogen-blending and system scale-up on the performance and economic viability of $\mathrm{CH_4}$ fueled SOFC systems, considering different gas path configurations and a technoeconomic assessment. The study introduced a kinetic approach for carbon deposition recognition and volume flow dependent pressure loss correlations. The key parameters energy input, pressure losses, and carbon deposition were identified, and their effects on operational safety, system performance, and economic viability were analyzed separately to resolve inconsistencies in previous studies on hydrogen blending and scale-up.

The optimal choice of the system parameters depends on the fuel feed composition and is constrained by the deposition of carbon and temperature limits. Introducing hydrogen into the CH_4 feed reduces the electrical efficiency for constant RR-RU-sets but mitigates CD, enabling operation points that compensate efficiency losses. On the other hand, pressure losses are increased by higher volume flows of hythane and affect the choice of the gas path configuration for the large-scale systems. Parallel configurations exhibit the lowest pressure loss and highest efficiencies.

Scaling up reduces the specific system costs by 91.7 %, from 2.41 $\[mathcal{\epsilon}\]$ /kWh to 0.20 $\[mathcal{\epsilon}\]$ /kWh, primarily due to strongly reduced capital costs. While the large-scale system is cost competitive with market prices for electricity, the small-scale system remains unprofitable. The cost increase for enabling $\[mathbb{H}_2\]$ admixture flexibility is low with 1.6 % for hardware adjustments and running on 30 vol% $\[mathbb{H}_2\]$.

The zero-dimensional cell model does not capture temperature or gas composition gradients, limiting its ability to reflect voltage variations across multi-stack systems. In addition, the steady-state Aspen model neglects fuel cell degradation and gas distribution. Future work should investigate start-up, shutdown, and load change strategies using higher-dimensional models that incorporate degradation mechanisms.

This study shows that hydrogen blending and parameter optimization can improve SOFC efficiency while maintaining technical feasibility. The results highlight the potential of SOFCs for industrial decarbonization and integration into future hydrogen infrastructures.

CRediT authorship contribution statement

Robert Styn: Writing – original draft, Visualization, Validation, Software, Methodology, Investigation, Conceptualization, Hannes Jakob Reichelt: Writing – review & editing, Visualization, Software, Methodology, Investigation. Ralf Peters: Writing – review & editing, Supervision, Thomas Ernst Müller: Writing – review & editing, Supervision.

Declaration of competing interest

The authors declare that they have no known competing financial

interests or personal relationships that could have appeared to influence the work reported in this paper.

Acknowledgments

The authors are grateful to their colleagues in the fuel synthesis departments at Jülich, as well as to all project and cooperation partners for the stimulating scientific exchange.

T.E.M. gratefully acknowledges funding of the endowed chair Carbon Sources and Conversion (CSC) by the state of North Rhine-Westphalia, grant number IRR-2018-1, RWE Power AG, and the Faculty of Mechanical Engineering of Ruhr-Universität Bochum.

Data availability

Data will be made available on request.

References

- [1] Wuebbles DJ, Fahey DW, Hibbard KA, DeAngelo B, Doherty S, Hayhoe K, et al. Executive Summary of the climate science special report: fourth national climate assessment, vol. I. Washington, DC, USA: U.S. Global Change Research Program; 2017. p. 470. https://doi.org/10.7930/J0J964J6.
- [2] IPCC. Summary for policymakers. In: Lee H, Romero J, editors. Climate change 2023: synthesis report. Contribution of working groups I, II and III to the sixth assessment report of the intergovernmental Panel on climate change [core writing team. Geneva, Switzerland: IPCC; 2023. p. 1–34. https://doi.org/10.59327/IPCC/ AR6-9789291691647.001.
- [3] International Energy Agency. Total energy supply (TES) by source. World; 1990-2021 2024. Available at: https://www.iea.org/data-and-statistics/data-tools/energy-statistics-data-browser?country=WORLD&fuel=Energy%20supply&indicator=TESbySource. [Accessed 12 August 2025].
- [4] Hermesmann M, Grübel K, Scherotzki L, Müller TE. Promising pathways: the geographic and energetic potential of power-to-x technologies based on regeneratively obtained hydrogen. Renew Sustain Energy Rev 2021;138:110644.
- [5] Tsiklios C, Schneider S, Hermesmann M, Müller TE. Efficiency and optimal load capacity of E-Fuel-Based energy storage systems. Adv Appl Energy 2023;10: 100140.
- [6] Hermesmann M, Müller TE. Green, turquoise, blue, or grey? Environmentally friendly hydrogen production in transforming energy systems. Prog Energy Comb 2022;90:100996
- [7] Hermesmann M, Tsiklios C, Müller TE. The environmental impact of renewable hydrogen supply chains: local vs. remote production and long-distance hydrogen transport. Appl Energy 2023;351:121920.
- [8] Tsiklios C, Hermesmann M, Müller TE. Hydrogen transport in large-scale transmission pipeline networks: thermodynamic and environmental assessment of repurposed and new pipeline configurations. Appl Energy 2022;327:120097.
- [9] Mitteilung der Kommission an das Europäische Parlament, den Rat. den Europäischen Wirtschafts- und Sozialausschuss und den Ausschuss der Regionen. 2020. Available at: https://eur-lex.europa.eu/legal-content/DE/ALL/? uri=CELEX:52020DC0067.
- [10] European Hydrogen Backbone. Implementation roadmap cross border projects and costs update. Available at: https://ehb.eu/files/downloads/EHB-2023-Impl ementation-Roadmap-Part-1.pdf. [Accessed 12 August 2025].
- [11] Mahant B, Linga P, Kumar R. Hydrogen economy and role of hythane as a bridging solution: a perspective review. Energy & Fuels 2021;35:15424–54.
- [12] Balakrishnan NK, Chelladorai P, Briggs HWG. A perspective on hythane fuel for a sustainable future. SAE Int J Sustain Transp Energy Environ Policy 2022;3.
- [13] Wasserstoff in der Gasinfrastruktur: DVGW/Avacon-Pilotvorhaben mit bis zu 20 Vol.-% Wasserstoff-Einspeisung in Erdgas H2-20. 2023.
- [14] Davis M, Okunlola A, Di Lullo G, Giwa T, Kumar A. Greenhouse gas reduction potential and cost-effectiveness of economy-wide hydrogen-natural gas blending for energy end uses. Renew Sustain Energy Rev 2023;171:112962.
- [15] Yoon D, Kim J, Kim DH, Hong J. Elucidating the sensitivity to key operating parameters of a commercial-scale solid oxide fuel cell stack with open cathode manifolds. Energy Conv Manag 2023;283:116934.
- [16] The fuel cell industry review 2021. 2021. Available at: https://www.erm.com/globalassets/documents/fuel-cell-industry-review/thefuelcellindustryreview2021.pdf. [Accessed 12 August 2025].
- [17] The fuel cell industry review 2022. 2022. Available at: https://www.erm.com/contentassets/55c43361e857413387f28fbacea6e91a/the-fuel-cell-industry-review-2022.pdf. [Accessed 12 August 2025].
- [18] Führen D, Myron G, Léonard K, Jan I, Martin R, Patrick W, et al. Wertschöpfungskette brennstoffzelle: Metastudie. Available at: https://www.now-gmbh.de/wp-content/uploads/2022/08/NOW_Wertschoepfungskette-Brennstoff zelle.pdf. [Accessed 12 August 2025].
- [19] Ldt Tanalyze. Solid oxide fuel cell market research report. 2023.
- [20] Global Market Insights. Fuel cell market report, 2024-2032. Available at: https://www.gminsights.com/industry-reports/fuel-cell/77. [Accessed 12 August 2025].

- [21] Energy B. The bloom energy server. 2023.
- [22] Stationary fuel cell: Bosch plans to start full-scale production in 2024: Alliance with Ceres Power intensified.
- [23] Schwarz M. SOFC in serie: bosch erhält 160 Mio. Förderung für Brennstoffzellen. 2023. Available at: https://h2-news.de/wirtschaft-unternehmen/sofc-in-serie-bosch-erhaelt-160-mio-e-foerderung-fuer-brennstoffzellen/;2023 [accessed 12 August 2025].
- [24] Ceres P. Weichai, Bosch and Ceres plan strategic collaboration for the Chinese market. 2022. https://www.ceres.tech/news/weichai-bosch-and-ceres-plan-strategic-collaboration-for-the-chinese-market/; [Accessed 12 August 2025].
- [25] Bienert C, Brandner M, Skrabs S, Venskutonis A, Sigl LS, Megel S, et al. CFY-stack technology: the next design. ECS Trans 2015;68:2159–68.
- [26] Fontell E, Mihails K, Stefan S. Strong partners in SOFC technology. 2015.
- [27] FuelCell Energy I. Solid oxide fuel cell: 250 kW fuel cell. 2022.
- [28] DeBellis C. 19th SOFC annual workshop LG fuel Cell Systems Inc. LG Fuel Cell Systems Inc.; 2018.
- [29] Funk J. LG Fuel Cell Systems quitting Ohio after receiving \$18 million in state and federal grants. The Plain Dealer - Cleveland, Ohio Newspaper; 2018.
- [30] Mitsubishi Heavy Industries L. Market introduction status of fuel cell System MEGAMIE and future efforts. 2021.
- [31] Deseure J, Bultel Y, Dessemond L, Siebert E. Theoretical optimisation of a SOFC composite cathode. Electrochim Acta 2005;50:2037–46.
- [32] Zhu W, Ding D, Xia C. Enhancement in three-phase boundary of SOFC electrodes by an ion impregnation method: a modeling comparison. Electrochem Solid State Lett 2008:11:B83.
- [33] Gong C, Luo X, Tu Z. Performance evaluation of a solid oxide fuel cell multi-stack combined heat and power system with two power distribution strategies. Energy Conv Manag 2022;254:115302.
- [34] Araki T, Ohba T, Takezawa S, Onda K, Sakaki Y. Cycle analysis of planar SOFC power generation with serial connection of low and high temperature SOFCs. J Power Sources 2006;158:52–9.
- [35] Piroonlerkgul P, Kiatkittipong W, Wongsakulphasatch S, Aiouache F, Assabumrungrat S. Evaluation of performance and operation viability of nonuniform potential solid oxide fuel cell fueled by reformed methane. J Power Sources 2014;246:719–28.
- [36] Kupecki J, Skrzypkiewicz M, Wierzbicki M, Stepien M. Experimental and numerical analysis of a serial connection of two SOFC stacks in a micro-CHP system fed by biogas. Int J Hydrogen Energ 2017;42:3487–97.
- [37] Pirasaci T. Non-uniform, multi-stack solid oxide fuel cell (SOFC) system design for small system size and high efficiency. J Power Sources 2019;426:135–42.
- [38] Hollmann J, Fuchs M, Spieker C, Gardemann U, Steffen M, Luo X, et al. System simulation and analysis of an LNG-fueled SOFC system using additively manufactured high temperature heat exchangers. Energies 2022;15.
- [39] Micoli L, Russo R, Coppola T, Pietra A. Performance assessment of the heat recovery system of a 12 MW SOFC-based generator on board a cruise ship through a 0D model. Energies 2023;16.
- [40] Powell M, Meinhardt K, Sprenkle V, Chick L, McVay G. Demonstration of a highly efficient solid oxide fuel cell power system using adiabatic steam reforming and anode gas recirculation. J Power Sources 2012;205:377–84.
- [41] Bai X, Luo L, Huang B, Huang Z, Jian Q. Flow characteristics analysis for multi-path hydrogen supply within proton exchange membrane fuel cell stack. Appl Energy 2021;301:117468.
- [42] Othman AM, El-Fergany AA. Optimal dynamic operation and modeling of parallel connected multi-stacks fuel cells with improved slime mould algorithm. Renew Energ 2021;175:770–82.
- [43] Li Q, Cai L, Yin L, Wang T, Li L, Xie S, et al. An energy management strategy considering the economy and lifetime of multistack fuel cell hybrid system. IEEE Transactions on Transportation Electrification 2023;9:3498–507.
- [44] Wang Z, Liu G, Liu X-b, Xiang H-f, Sun C, Wang Z, et al. Inconsistency analysis and power allocation of the stack in multi-stack solid oxide fuel cell system. J Power
- power allocation of the stack in multi-stack solid oxide fuel cell system. J Power Sources 2024;598:234163.[45] Dépature C. Simulation model of a multi-stack fuel cell system. 2013, 6634727.
- [46] Marx N, Cardozo J, Boulon L, Gustin F, Hissel D, Agbossou K. Comparison of the series and parallel architectures for hybrid multi-stack fuel cell battery systems.
- Ieee Vehicle Power 2015:1–6.

 [47] Vivanpatarakij S, Assabumrungrat S, Laosiripojana N. Improvement of solid oxide fuel cell performance by using non-uniform potential operation. J Power Sources

2007:167:139-44.

- [48] Assabumrungrat S, Ruangrassamee N, Vivanpatarakij S, Laosiripojana N, Arpornwichanop A. Influence of stack arrangement on performance of multiplestack solid oxide fuel cells with non-uniform potential operation. J Power Sources 2009:187:1-7.
- [49] Tomberg M, Heddrich MP, Metten M, Ansar SA, Friedrich KA. Operation of a solid oxide fuel cell reactor with multiple stacks in a pressured system with fuel gas recirculation. Energy Technol 2022;10:202101075.
- [50] Qin HC, Cheng Z, Zhang BT, Zhou RJ, Yu YW, Li X, et al. Thermoelectrical comprehensive analysis and optimization of multi-stack solid oxide fuel cell system. Energy Conv Manag 2023;291:117297.
- [51] Buchinger G, Kraut J, Raab T, Griesser S, Lawlor V, Haiber J, et al. Operating micro-tubular SOFCs containing nickel based anodes with blends of methane and hydrogen. 2007. 450-455.

- [52] Panagi K, Laycock CJ, Reed JP, Guwy AJ. The effects of fuel variability on the electrical performance and durability of a solid oxide fuel cell operating on biohythane. Int J Hydrogen Energ 2021;46:2630–45.
- [53] Panagi K, Laycock CJ, Reed JP, Guwy AJ. Highly efficient coproduction of electrical power and synthesis gas from biohythane using solid oxide fuel cell technology. Appl Energy 2019;255:113854.
- [54] Simic K, Van Nieuwenhuyse J, De Paepe M. Experimental performance analysis of a fuel cell unit for various natural gas-hydrogen fuel mixtures. Am Soc Therm Fluids Eng (ASTFE) 2022:450–5.
- [55] Cinti G, Bidini G, Hemmes K. Comparison of the solid oxide fuel cell system for micro CHP using natural gas with a system using a mixture of natural gas and hydrogen. Appl Energy 2019;238:69–77.
- [56] Veluswamy GK, Laycock CJ, Shah K, Ball AS, Guwy AJ, Dinsdale RM. Biohythane as an energy feedstock for solid oxide fuel cells. Int J Hydrogen Energ 2019;44: 27896–906.
- [57] Hai T, El-Shafay AS, Alizadeh Aa, Dhahad HA, Chauhan BS, Almojil SF, et al. Comparison analysis of hydrogen addition into both anode and afterburner of fuel cell incorporated with hybrid renewable energy driven SOFC: an application of techno-environmental horizon and multi-objective optimization. Int J Hydrogen Energ 2024;51:1195–207.
- [58] Hormaza Mejia A, Yoshioka M, Kim JY, Brouwer J. Impacts of hydrogen-natural gas mixtures on a commercial solid oxide fuel cell system. ECS Trans 2020;96: 133–48.
- [59] Payne R, Love J, Kah M. Generating electricity at 60% electrical efficiency from 1 -2 kWe SOFC products. ECS Trans 2009;25:231–9.
- [60] Peters R, Deja R, Blum L, Pennanen J, Kiviaho J, Hakala T. Analysis of solid oxide fuel cell system concepts with anode recycling. Int J Hydrogen Energ 2013;38: 6809–20
- [61] Doherty WG, Reynolds A, Kennedy D. Modelling and simulation of a biomass gasification-solid oxide fuel cell combined heat and power plant using aspen plus. 2009.
- [62] Leonide A, Apel Y, Ivers-Tiffee E. SOFC modeling and parameter identification by means of impedance spectroscopy. ECS Trans 2009;19:81–109.
- [63] Grosselindemann C, Russner N, Dierickx S, Wankmüller F, Weber A. Deconvolution of gas diffusion polarization in Ni/Gadolinium-doped ceria fuel electrodes. J Electrochem Soc 2021;168:124506.
- [64] Achenbach E, Riensche E. Methane steam reforming kinetics for solid oxide fuelcells. J Power Sources 1994;52:283–8.
- [65] Aguiar P, Adjiman CS, Brandon NP. Anode-supported intermediate temperature direct internal reforming solid oxide fuel cell. I: model-based steady-state performance. J Power Sources 2004;138:120–36.
- [66] Schäfer F, Egger S, Steiner D, Carré M, Eichel R-A. Control of oxygen-to-carbon ratio and fuel utilization with regard to solid oxide fuel cell systems with anode exhaust gas recirculation: a review. J Power Sources 2022;524:231077.
- [67] Corigliano O, Pagnotta L, Fragiacomo P. On the technology of Solid Oxide Fuel Cell (SOFC) energy systems for stationary power generation: a review. Sustainability 2022:14:15276.
- [68] Slycke JT, Mittemeijer EJ, Somers MAJ. Thermodynamics and kinetics of gas and gas-solid reactions of chapter. In: Thermodynamics and kinetics of gas and gas-solid reactions of book. Elsevier; 2015. p. 3–111.
- [69] Snider DM, Clark SM, O'Rourke PJ. Eulerian–Lagrangian method for threedimensional thermal reacting flow with application to coal gasifiers. Chem Eng Sci 2011;66:1285–95.
- [70] Biert Lv, Visser K, Aravind PV. A comparison of steam reforming concepts in solid oxide fuel cell systems. Appl Energy 2020;264:114748.
- [71] Turton R, Bailie R, Whiting W, Shaeiwitz J, Bhattacharyya D. Analysis, synthesis, and design of chemical processes. Boston: Prentice Hall; 2018.
- [72] Battelle Memorial I. Manufacturing cost analysis of 1, 5, 10 and 25 kW fuel cell systems for primary power and combined heat and power applications. 2017.
- [73] Battelle Memorial I. Manufacturing cost analysis of 100 and 250 kW fuel cell systems for primary power and combined heat and power applications. 2016.
- [74] GmbH EBC. Hydex & HydexPLUS Kostenindizes für Wasserstoff: unsere belastbare Entscheidungsgrundlage für Ihre Investitions-entscheidung in der Wasserstoff-wirtschaft. Available at: https://e-bridge.de/kompetenzen/wasser stoff/h2index. [Accessed 7 July 2024].
- [75] Destatis Statistisches B. Erdgas- und Stromdurchschnittspreise: Tabellen. Available at: https://www.destatis.de/DE/Themen/Wirtsch aft/Preise/Erdgas-Strom-DurchschnittsPreise/_inhalt.html#421258. [Accessed 7 July 2024].
- [76] Riegraf M, Bombarda I, Domling F, Liensdorf T, Sitzmann C, Langhof N, et al. Enhancing the mechanical strength of electrolyte-supported solid oxide cells with thin and dense Doped-Ceria interlayers. ACS Appl Mater Interfaces 2021;13: 49879–89.
- [77] Engelbracht M, Peters R, Blum L, Stolten D. Analysis of a solid oxide fuel cell system with low temperature anode off-gas recirculation. J Electrochem Soc 2015; 162:F982–7
- [78] BDEW. Strompreisanalyse. Available at: https://www.bdew.de/service/daten-und-grafiken/bdew-strompreisanalyse/.
- [79] Berger B. Advancing europes energy systems: stationary fuel cells in distributed generation. Available at: https://www.clean-hydrogen.europa.eu/document/do wnload/8d78fca2-8507-4678-867c-548cd03ffb15_en?filename=FCHJU_FuelCell DistributedGenerationCommercialization.pdf. [Accessed 12 August 2025].